Supplementary Material for "Fermi surface and mass renormalization in the iron-based superconductor YFe_2Ge_2"

This material details quantum oscillation results not shown in the main paper, including de Haas-van Alphen traces obtained in S2, in which $\hat{a}$ is aligned with the axis of the pickup coil, and a Dingle analysis of the mean free paths in S1 and S2. It also provides a brief account of the origin of the magnetic torque interaction, which in the main paper is shown to produce clear quantum oscillation signatures attributable to the electron pocket in YFe_2Ge_2.

FURTHER QUANTUM OSCILLATION DATA

Sample S2

In the main de Haas-van Alphen study carried out on the Cambridge cryomagnet facility, two samples were mounted on the same rotation mechanism, one (S1) with $\hat{c}$ aligned with the pickup coil and the other (S2) with the $\hat{a}$ axis aligned with the axis of the pickup coil. Because both pickup coils were approximately parallel to each other, the angles between the applied field and the crystallographic $\hat{c}$ direction are related roughly by $\theta_{S2} = 90° - \theta_{S1}$, although a further small correction was necessary to account for misalignments within the rotation mechanism. Figure 3 in the main paper shows distinct quantum oscillations recorded in sample S1. In S2, quantum oscillations could also clearly be observed (Fig. S1), but with reduced signal-to-noise ratio compared to the data obtained in S1. We attribute the smaller signal-to-noise ratio in S2 largely to a lower mean free path than in S1, as is evaluated in the following section.

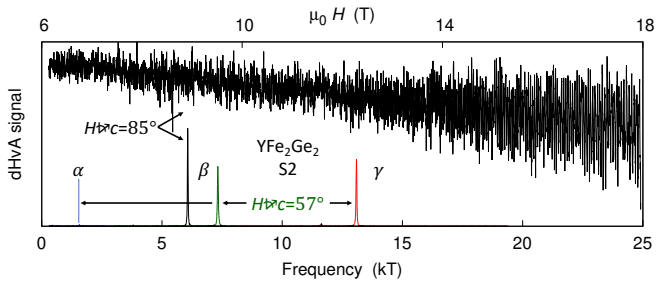

Figure S1. Typical de Haas-van Alphen data obtained in sample 2 (S2) of YFe_2Ge_2: oscillations are weaker than in S1 (Fig. 3 in main paper), but signatures of the three hole pockets can be resolved at most orientations.

Dingle analysis

Mean free paths can be estimated from the dependence of the quantum oscillation (QO) amplitude on applied field B by using the standard Dingle analysis (e.g. [1]). We assume that the QO contribution at each frequency has an amplitude given by Lifshitz-Kosevich theory as

$$\tilde{y} \propto \frac{X}{\sinh X} \frac{e^{-B_0/B}}{B^{3/2}} \quad , \tag{1}$$

where B_0 specifies the primary field dependence and $X = \pi^2 \frac{m^*}{m_e} \frac{k_B T}{\mu_B B}$. The $X/\sinh(X)$ term introduces the dependence on temperature T, which is used in the main part of the paper to extract the ratio of effective mass m^* over bare electron mass m_e. The field scale B_0 relates to the quasiparticle scattering rate τ^{-1} via $B_0/B = \pi/(\omega_c \tau)$, where $\omega_c = eB/m^*$ is the cyclotron frequency, as $\tau^{-1} = B_0 e/(\pi m^*)$. The mean free path follows as $\ell = v_F \tau$. The Fermi velocity v_F is linked to the Fermi wavevector k_F by $v_F = \hbar k_F / m^*$. We extract k_F from the measured QO frequency F via the Onsager relation, giving an expression for ℓ that does not depend on the effective mass m^*:

$$\ell = \frac{\pi}{B_0} \sqrt{2\hbar F / e} \quad . \tag{2}$$

We obtain estimates of ℓ for samples S1 and S2 by choosing a rotation angle at which high quality data was recorded and at which a single frequency is most

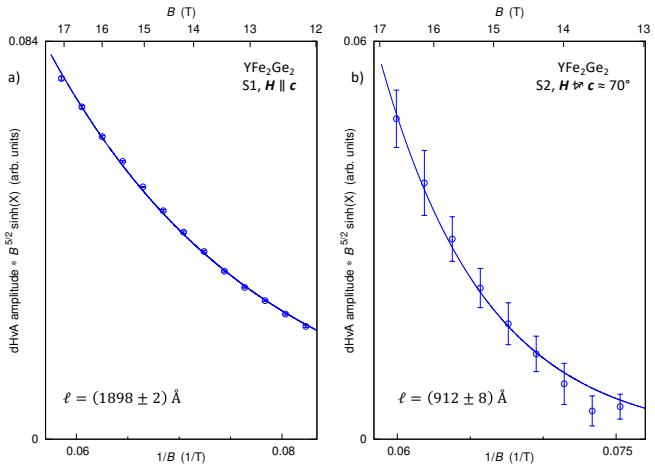

Figure S2. QO Dingle analysis of mean free paths in YFe_2Ge_2. **(a)** For sample S1 ($\ell \simeq 1898(2)$ Å), using oscillations at the β frequency and **(b)** for sample S2 ($\ell \simeq 912(8)$ Å), using oscillations at the γ frequency.

prominent. The contribution from this frequency was extracted by applying a band-pass filter with passband width 200 T. The envelope was determined from the maxima of these oscillations by averaging over a narrow field interval. The resulting envelope $\tilde{y}(B)$ was multiplied with $B^{5/2}\sinh X$, where X can be calculated from the effective mass previously determined by analyzing the T-dependence of oscillation amplitudes (see main paper), producing the data summarized in Fig. S2. An exponential decay of the form $e^{-B_0/B}$ was fitted to these data, resulting in estimated mean free paths of the order of 1900 Å for S1 and 900 Å for S2.

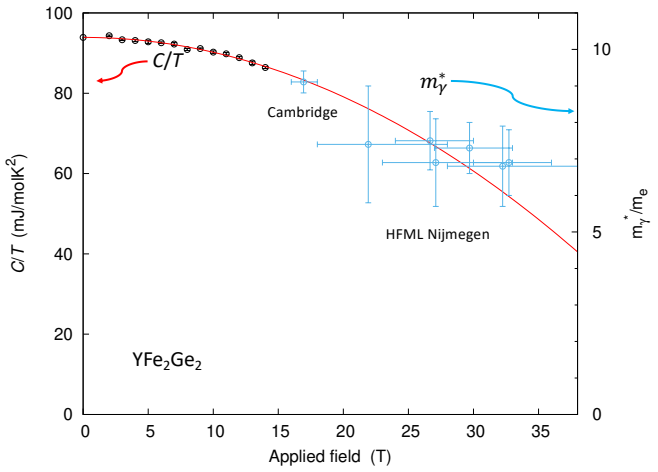

Figure S3. Field dependence of QO masses (blue circles with errorbars) extracted at a field angle $\theta = 70°$ for oscillations arising from the $\gamma-$orbit in Cambridge measurements at up to 18 T and in higher field measurements at HFML Nijmegen. Horizontal errorbars indicate the field range over which the LK-form was applied to extract a mass estimate. The downward trend of masses vs. applied field is compared to the field dependence of the Sommerfeld ratio of the heat capacity C/T determined at $T = 1.5$ K in fields of up to 14 T (black circles). The red line indicates the result of a parabolic fit to the C/T data, extrapolated to higher fields.

Field dependence of effective masses

The dependence of the Sommerfeld ratio C/T on applied magnetic field shown in the inset of Fig. 4a of the main paper suggests that quasiparticle effective masses are reduced in applied field. A reduction by about 20% at fields of about 18 T would be consistent with the discrepancy between the zero-field $C/T \simeq 95\,\mathrm{mJ/molK^2}$ and the DFT prediction renormalised by a uniform mass enhancement of 4.7 determined in the field range 16−18 T, which would give $C^*/T \simeq 76\,\mathrm{mJ/molK^2}$. Figure S3 shows the field dependence of the Sommerfeld ratio and effective masses on the $\gamma-$orbit, extracted from QO measurements at a field angle of $\theta = 70°$ in fields beyond 18 T in the resistive magnet system at HFML Nijmegen and at up to 18 T shown in the main paper. The comparison between the HFML Nijmegen data and the lower field Cambridge data suggests that the trend indicated by heat capacity measurements in field, namely that quasiparticle masses are reduced in high applied fields, continues beyond 20 T, although with a weaker field dependence. This preliminary study suffers from large error bars on the quasiparticle masses extracted from the highest field QO measurements. A more detailed investigation of the field dependence of effective masses on all orbits and to lower fields that overlap with the range of the heat capacity measurements will be required to pin down the origin of the $\simeq 20\%$ discrepancy between zero-field Sommerfeld ratio and the effective masses observed at $\simeq 18$ T.

MAGNETIC TORQUE INTERACTION

The response of a torque cantilever in high magnetic fields is complicated by the fact that the bending of the cantilever itself changes the angle between the applied field and the sample. Quantum oscillations at one frequency F_1 thereby cause a modulation in the effective angle which is overlaid with oscillations at a second frequency F_2. This causes sum- and difference-frequencies $F_1 \pm F_2$ to appear in the QO power spectrum. The 'torque interaction' phenomenon is discussed in detail in [1, 2].

To illustrate this effect, we note that the oscillatory torque $\tilde{\tau}$ is given by the oscillatory magnetisation $\tilde{M}_t$ transverse to the applied field B as

$$\tilde{\tau} = \tilde{M}_t B \quad . \tag{3}$$

For a single oscillatory component, the oscillatory transverse magnetization, in turn, is related to the oscillatory longitudinal magnetization $\tilde{M}_\ell$ via $\tilde{M}_t = -\frac{1}{F}\frac{\partial F}{\partial \theta}\tilde{M}_\ell$, where F is the QO frequency and θ is the rotation angle of the sample. More generally, the longitudinal and transverse magnetization contain quantum oscillations over a discrete set of frequencies F_i.

Because $\tilde{M}_t$ in Eqn. 3 itself depends on θ via the θ dependence of the QO frequencies, and θ depends on the torque, we need to consider the feedback effect on the torque. The torque causes the angle between sample and field to change from the angle θ_0 set by the rotation mechanism to a new angle $\theta = \theta_0 + \alpha\tau$ to first order in τ, where α depends on the stiffness of the cantilever. This results in an implicit equation for the observed torque at the actual angle θ, which can be expanded to first order and thereby related to the torque that would have been present at the angle θ_0 set by the rotation mechanism, as:

$$\tau(\theta) = \tau(\theta_0 + \alpha\tau) \simeq \tau(\theta_0)\left(1 + \alpha\frac{\partial\tau}{\partial\theta}\right) \quad . \tag{4}$$

The nonlinearity which mixes QO frequencies arises from the product $\tau\frac{\partial\tau}{\partial\theta}$ in Eqn. 4. Writing the oscillatory

contributions to $\tau(\theta_0)$, or to $\tau(\theta)$ in the limit of infinite cantilever stiffness, as

$$\tilde{\tau}(\theta_0) = \sum_i R_i \sin\left(\frac{2\pi F_i}{B} + \phi_i\right) \tag{5}$$

and dropping the phase-shifts ϕ_i, we find for the actual observed torque at finite cantilever stiffness

$$\begin{aligned}\tilde{\tau}(\theta) = &\sum_i R_i \sin\left(\frac{2\pi F_i}{B}\right) + \\ &\frac{\alpha\pi}{B}\sum_{ij} R_i R_j \frac{\partial F_j}{\partial\theta}\sin\left(\frac{2\pi}{B}(F_i + F_j)\right) + \\ &\frac{\alpha\pi}{B}\sum_{ij} R_i R_j \frac{\partial F_j}{\partial\theta}\sin\left(\frac{2\pi}{B}(F_i - F_j)\right) \quad .\end{aligned} \tag{6}$$

The measured oscillatory torque therefore shows oscillations not only at the fundamental frequencies F_i but also at sum and difference frequencies $F_i \pm F_j$. If the analysis is extended beyond first order in Eqn. 4, a comb of frequencies $F_i \pm nF_j$ will be obtained, as was indeed observed in some high field runs in YFe_2Ge_2. More dramatic effects of the torque interaction such as instabilities and hysteresis phenomena are beyond this analysis and were not observed in our high field measurements.

[1] D. Shoenberg, *Magnetic Oscillations in Metals*, 1st ed. (Cambridge University Press, Cambridge, 1984).

[2] J. Vanderkooy and W. R. Datars, Effects of sample rotation on de Haas – van Alphen oscillations, Can. J. Phys. **46**, 1215 (1968).